Journal of Applied Polymer Science

Self-nucleation behaviors of olefinic blocky copolymer/montmorillonite nanocomposites with collapsed and intercalated clay layers

Zai-Zai Tong, Jie Huang, Bing Zhou, Jun-Ting Xu, Zhi-Qiang Fan

MOE Key Laboratory of Macromolecular Synthesis and Functionalization, Department of Polymer Science and Engineering, Zhejiang University, Hangzhou 310027, China

Correspondence to: J.-T. Xu (E-mail: xujt@zju.edu.cn)

ABSTRACT: The self-nucleation behavior of olefinic blocky copolymer (OBC) / organically modified montmorillonite (OMMT) nanocomposites with a novel collapsed clay structure (c-OMMT) was studied and compared with that of the nanocomposites with an intercalated clay structure (OBC/i-OMMT). Their behaviors appear different in three temperature domains, Domain I (D_I) in which the polymer is completely melted and only the heterogeneous nuclei are present, Domain II (D_{II}) in which only self-nucleation occurs and Domain III (D_{III}) where both self-nucleation and annealing take place. As the OMMT loading increases, the boundary temperature of D_I and D_{II} ($T_{I\rightarrow II}$) shifts to lower temperature and D_{II} becomes narrower. For the OBC/c-OMMT nanocomposites, the $T_{I\rightarrow II}$ or $T_{I\rightarrow III}$ (the boundary temperature of D_I and D_{III}) can be lower than the end melting temperature (T_m^{end}) and leads to appearance of a subdomain of D_I, D_I', in which the self-nuclei of un-melted fragmental crystals exist but the following crystallization is still initiated by c-OMMT. D_{II} may even disappear at high c-OMMT loadings. By contrast, the $T_{I\rightarrow II}$ of the OBC/i-OMMT nanocomposites is always approximate to or higher than the T_m^{end}. D_{II} does not disappear and no D_I' is observed for the OBC/i-OMMT nanocomposites. The nucleation efficiency of c-OMMT is also evidently higher than that of i-OMMT. These results verify that the c-OMMT has stronger nucleation ability than i-OMMT at the same OMMT loading. © 2014 Wiley Periodicals, Inc. J. Appl. Polym. Sci. **2015**, *132*, 41771.

KEYWORDS: clay; composites; crystallization; differential scanning calorimetry (DSC); polyolefins

Received 15 September 2014; accepted 18 November 2014

DOI: 10.1002/app.41771

INTRODUCTION

In the past two decades, much attention has been paid to polymer/clay nanocomposites, because these materials offer markedly improved properties as compared to the base materials, which can be attributed to the high aspect ratio of the clay layers and the strong interaction between the polymer matrix and the clay surface.[1–3] When the polymer is crystallizable, the nanoclay can also affect the crystallization behavior, such as crystallization kinetics, nucleation and even the crystal structure of the polymer.[4–6] On the other hand, crystallization behavior of the polymer and thus the properties of the nanocomposites are strongly dependent on the dispersion state of nanoclay.[7–10] For instance, aggregated clay layers have only a limited effect on the polymer crystallization due to the weak affinity to polymer matrix.[7,8] By contrast, the completely exfoliated clay layers may exhibit a strong nucleation effect on polymer crystallization, resulting in enhanced crystallization rate and smaller size of spherulites,[9,10] whereas intercalated clay layers might simultaneously exert nucleation and retardance effects on polymer crystallization.[9,10] Therefore, it is of great importance to investigate the clay dispersion and its effect on the crystallization behavior and mechanical properties of clay-based nanocomposites.

Olefinic blocky copolymer (OBC) is a new type of thermoplastic elastomer with a multi-block structure comprising hard blocks having very low octene content and high melting temperature and soft blocks with almost no crystallinity.[11–18] In our previous work, the nanocomposites of OBC and organically modified montmorillonite (OMMT) with a novel collapsed clay structure (c-OMMT), which is rarely reported in literature,[19–21] were prepared by a solution-precipitation process.[8] We observed that the nuclei density of the OBC/c-OMMT nanocomposites was evidently higher than that of the nanocomposites containing intercalated OMMT (i-OMMT) layers.[8] The hierarchical structures from nano- to micro- levels of the OBC/c-OMMT and OBC/i-OMMT nanocomposites are quite different as well.[22] However, more in-depth investigations are needed to understand how the c-OMMT affects the nucleation of OBC, since it

Additional Supporting Information may be found in the online version of this article.

has a significant impact on the bulk properties and processability of polymer materials.

Self-nucleation (SN) method is a powerful method to probe the nucleation mechanism of semicrystalline polymers,[23–26] nanocomposites[27–30] and block copolymers,[31–35] which was first proposed by Fillon *et al.*[36] In this method, the polymer is first held at a high temperature for a certain time and then cooled at a constant rate to create a "standard state". Subsequently, the sample is heated to different self-nucleation temperatures (T_s) and held at T_s for a certain time. After self-nucleation, the sample is cooled from T_s to crystallize and then heated to melt. The nucleation behavior of a polymer can usually be divided into three domains. D_I is usually entered when T_s is slightly higher than the melting temperature (T_m) of the polymers, if the so-called "memory effect" is not pronounced. In D_I only thermally resistant nuclei (generally heterogeneous nuclei) exist and the number of nuclei is constant, so polymer always crystallizes at the same temperature if the same cooling rate is applied. Only self-nucleation occurs in Domain II (D_{II}), which is characterized by a drastic increase in nucleation density and a corresponding shift of the crystallization temperature (T_c) to higher temperatures upon cooling from T_s. At lower temperatures, both self-nucleation and annealing of the un-melted crystals take place, which is indicative of Domain III (D_{III}).

Although SN technique has been applied for polymer nanocomposites to study the nucleation behavior of the nano-fillers, the nucleation ability of the same nano-fillers with different dispersion states has never been compared before. In the present work, we investigated the self-nucleation behaviors of OBC/c-OMMT and OBC/i-OMMT nanocomposites with various OMMT loadings. Since a "standard state" is first created in the SN experiment, the nucleation ability of c-OMMT and i-OMMT toward crystallization of OBC in D_I can be evaluated with that of the self-nuclei in D_{II} as a reference. The result revealed that c-OMMT and i-OMMT exhibited a remarkable difference in nucleation ability. This will lead to better understanding the effect of clay dispersion state on polymer crystallization and further approaching control and regulation of the morphology and properties of semicrystalline polymer/clay nanocomposites.

EXPERIMENTAL

Materials and Sample Preparation

The ethylene-octene blocky copolymer (OBC) was kindly supplied as pellets by the Dow Chemical Company. The weight-average molecular mass and the polydispersity (M_w/M_n) of OBC are 90 kg/mol and 3.1, respectively. The overall octene content in OBC is 13.2 mol %. Montmorillonite organically modified with dimethyl dehydrogenated tallow ammonium (OMMT, brand: Nanomer 1.44P) was purchased from Nonocor (USA). The OBC/OMMT nanocomposites with intercalated and collapsed clay structures (OBC/i-OMMT and OBC/c-OMMT) were prepared according to the procedures reported in our previous work.[8] Firstly, the OBC was dissolved in xylene solution at 120°C with a concentration of 1.0 w/v %. On the other hand, the OMMT was dispersed in xylene and sonicated for 60 min at room temperature. The OMMT/xylene mixture was slowly added into the OBC/xylene solution. After further stirring for 6 h, the hot solution was poured into excess ethanol, and OBC and OMMT were co-precipitated from the solution. The obtained nanocomposites have a collapsed clay structure. Such nanocomposites with different OMMT loadings are named as OBC/c-OMMT-*x*, where *x* represents the weight percentage of OMMT. By contrast, the nanocomposites having an intercalated clay structure with an OMMT loading of *x* wt % (named as OBC/i-OMMT-*x*) were prepared by directly evaporating the solvent, xylene, at 60°C. The OMMT loadings in both OBC/c-OMMT and OBC/i-OMMT nanocomposites are 0.5, 1.0, 2.0, 3.0 wt %, respectively. The collapsed and intercalated structures of c-OMMT and i-OMMT in the nanocomposites were verified with different techniques.[8,22]

SN Experiments

Self-nucleation (SN) experiments were performed on a TA Q200 differential scanning calorimeter (DSC) under nitrogen. The sample was encapsulated in an aluminum pan and the sample weight was about 3–5 mg. The temperature profile for SN experiments was shown in Figure S1 in Supporting Information, which was originally devised by Fillon *et al.*[36] The complete thermal treatment comprises following five steps: (a) The thermal history was first eliminated by heating the sample to 180°C and holding for 5 min, at which only the heterogeneous nuclei can survive. (b) A "standard" thermal history was created by cooling the samples to 40°C at a rate of 10°C/min. (c) The sample was heated to pre-set self-nucleation temperature (T_s) and held for 5 min. (d) Subsequently, the sample was cooled to 40°C for crystallization and (e) finally again heated to melt. The aforementioned five steps were repeated at different T_ss.

Polarized Optical Microscopy

Polarized optical microscopy (POM) observations at selected T_ss were carried out on an Olympus microscope (BX51) equipped with a hot stage. The thermal treatment was the same as the SN thermal protocol applied in the DSC experiment.

RESULTS AND DISCUSSION

SN of the Neat OBC

For the purpose of comparison, the SN behavior of the neat OBC was first studied. The DSC cooling traces of the neat OBC after self-nucleation at various T_ss and the subsequent melting traces are shown in Figure 1(a,b), respectively. It is observed that, when T_s is equal or higher than 163°C, the crystallization temperature (T_c) of the neat OBC is constant, irrespectively of T_s. The invariant T_c is the characteristic of Domain I (D_I), where only thermally resistant nuclei initiate crystallization of OBC. When T_s is below 163°C, T_c starts to increase gradually as T_s decreases, whereas there is no evidence of annealing on the subsequent melting trace. The increase of T_c with lowering T_s is the feature of Domain II (D_{II}), which is due to the stronger nucleation ability of the self-nuclei than the thermal resistant ones and more self-nuclei formed at lower temperatures. When T_s crosses 122°C, the crystallization peak of OBC becomes considerably weak, indicating that a larger fraction of OBC crystals are left and un-melted at such a low T_s. These un-melted crystals can undergo annealing to form more perfect crystals in the subsequent heating process, leading to appearance of a second

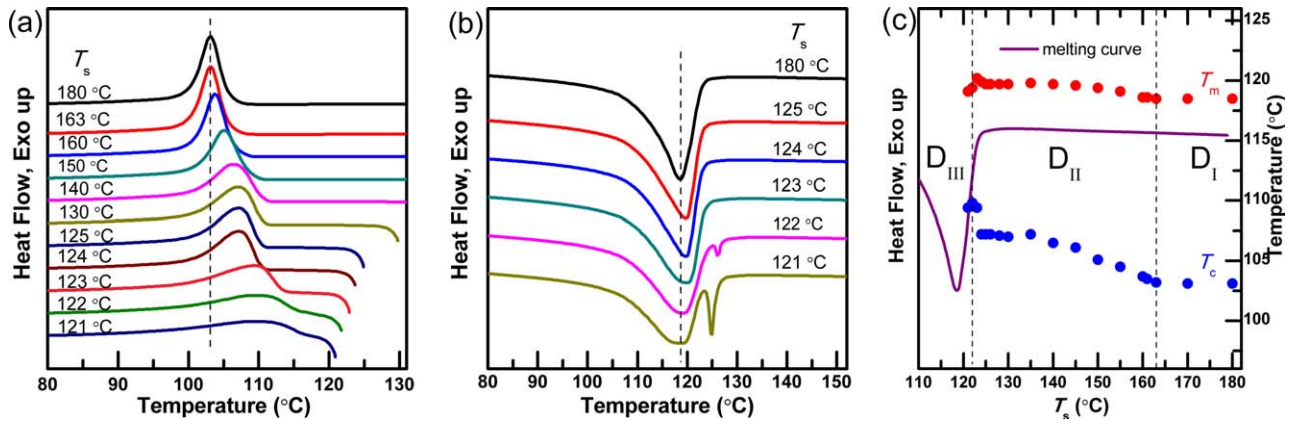

Figure 1. DSC cooling traces after self-nucleation at various T_ss (a), subsequent melting traces (b), variations of T_m and T_c with T_s and self-nucleation domains of the melting curve (divided by the vertical dashed lines) (c) of the neat OBC. [Color figure can be viewed in the online issue, which is available at wileyonlinelibrary.com.]

tiny melting peak at higher temperatures, which is the symbol of entry into Domain III (D_{III}). With further decrease of T_s, the shoulder melting peak at higher temperature becomes stronger. The data in Figure 1 show that D_I of the neat OBC is located at $\geq$163°C, D_{II} is between 163°C and 122°C, and D_{III} is $\leq$122°C, as summarized in Table I. The variations of T_c and T_m with T_s for the OBC are shown in Figure 1(c) and the three T_s domains divided by the dashed lines are indicated as well.

One can see from Figure 1 that the boundary temperature of D_I and D_{II} ($T_{I\to II}$, 163°C) of the neat OBC is much higher than the equilibrium melting temperature (T_m^0) of polyethylene (PE) homopolymer, which is 145.5°C.[37] Such an SN behavior is quite different from that reported for PE,[38] in which the $T_{I\to II}$ is close to the end melting temperature (T_m^{end}). According to Hu and coworkers, this intriguing phenomenon could be attributed to the retained molecular clusters in the melt, which is due to the segment segregation of different sequence lengths in ethylene/α-olefin random copolymers induced by previous crystallization.[39,40] These molecular clusters could act as self-nuclei in the following crystallization process,[41] leading to a higher $T_{I\to II}$. Moreover, these remained molecular clusters are thermodynamically stable in the melt, since their nucleation effect does not fade out with prolongation of annealing time in the melt, as shown in Supporting Information [Figure S2].

Table I. Temperature Ranges of the Various T_s Domains for all the Samples

Samples	D_I (°C)	D_I' (°C)	D_{II} (°C)	D_{III} (°C)
Neat OBC	≥ 163	-	163–122	≤ 122
OBC/c-OMMT-0.5	≥ 147	-	147–122	≤ 122
OBC/c-OMMT-1	≥ 127	-	127–122	≤ 122
OBC/c-OMMT-2	≥ 127	127-122	-	≤ 122
OBC/c-OMMT-3	≥ 127	127-123	-	≤ 123
OBC/i-OMMT-0.5	≥ 145	-	145–122	≤ 122
OBC/i-OMMT-1	≥ 138	-	138–122	≤ 122
OBC/i-OMMT-2	≥ 127	-	127–122	≤ 122
OBC/i-OMMT-3	≥ 125	-	125–122	≤ 122

Although the molecular clusters are stable in the melt, the T_s within D_{II} still has an influence on the concentration of the molecular clusters, since the molecular conformation is more approaching to equilibrated random coil at a higher T_s. More molecular clusters are formed at a lower T_s, leading to the increase of T_c with lowering T_s above the T_m. In the T_s range of 135–124°C, the T_c of OBC is nearly invariant, indicating a constant number of the self-nuclei, i.e. molecular clusters. Nevertheless, a sudden increase of T_c is observed in the T_s range of 124–122°C. Since the temperature of 124°C is lower than the T_m^{end} of OBC, thus partial fragmental crystals are un-melted, which can also serve as self-nuclei and lead to increase of T_c. As a result, there are two types of self-nuclei in the neat OBC: molecular clusters and un-melted fragmental crystals. The former mainly take effect in the melt above T_m^{end} and the latter nucleate crystallization when T_s is below T_m^{end}.

SN of the OBC/c-OMMT Nanocomposites

The dispersion state of clay layers in the polymer matrix was characterized by WAXD and TEM in our previous work,[8,22] since it is a crucial parameter towards polymer crystallization. It is found that the collapsed clay layers (c-OMMT) have a much smaller basal spacing (d_{001}) between the clay layers, while intercalated clay layers (i-OMMT) have a larger d_{001} than the original organically modified clay layers. Both types of the clay layers are well dispersed in the OBC matrix, as revealed by TEM.[8,22] The clay layers are densely stacked with more layers in per clay particle in the OBC/c-OMMT nanocomposites.[22] By contrast, the clay layers are loosely stacked in the OBC/i-OMMT nanocomposites due to intercalation of OBC chains, leading to fewer layers in per clay particle.[22] As a consequence, the surface area for nucleation of c-OMMT particles is much lower than that of i-OMMT at the same OMMT loading.[22] However, the crystallization temperature of OBC/c-OMMT is higher than that of OBC/i-OMMT.[22] Therefore, the nucleation ability of these two types of clay layer should be further explored by SN method.

As expected, after addition of OMMT, the SN behavior of OBC will certainly be altered because OMMT can act as

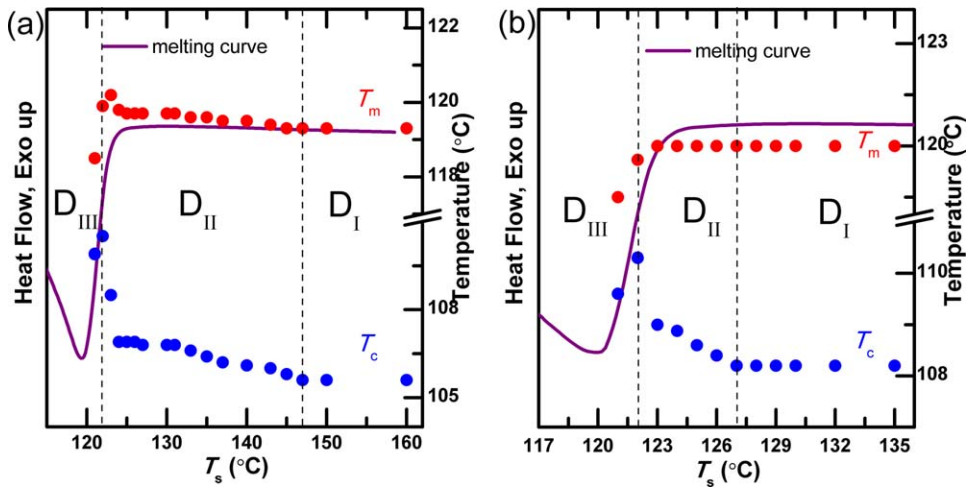

Figure 2. Variations of T_m and T_c with T_s and self-nucleation domains of the melting curve (divided by the vertical dashed lines) of OBC/c-OMMT-0.5 (a) and OBC/c-OMMT-1 (b). [Color figure can be viewed in the online issue, which is available at wileyonlinelibrary.com.]

heterogeneous (thermally resistant) nuclei to initiate crystallization. Here we first examine the SN behavior of OBC/c-OMMT nanocomposites. The variations of T_c and T_m with T_s and the temperature ranges of three domains for OBC/c-OMMT containing 0.5 wt % and 1.0 wt % c-OMMT are illustrated in Figure 2. The related data are summarized in Table I. The melting and cooling DSC traces at different T_ss are shown in Supporting Information [Figures S3 and S4]. It is observed that the T_c is invariant at T_s >147°C and starts to increase with lowering T_s at T_s <147°C for OBC/c-OMMT-0.5 [Figure 2(a)], thus the $T_{I\rightarrow II}$ is determined to be 147°C for this nanocomposite, which is lower than that of the neat OBC. As for the sample OBC/c-OMMT-1 with 1.0 wt % c-OMMT loading, the $T_{I\rightarrow II}$ further shifts to lower temperature, which is 127°C. Such a temperature is close to the T_m^{end} of OBC/c-OMMT-1 [Figure 2(b)]. The shift of $T_{I\rightarrow II}$ toward lower temperature is due to more heterogeneous nuclei at a higher clay loading.

It should be noted that, the number of the molecular clusters dramatically increases with lowering T_s, but the number of c-OMMT is constant in a given sample. The nucleation density in OBC/c-OMMT-0.5 and the neat OBC with lowering T_s could be confirmed by POM. Figure 3 illustrates the POM images of OBC/c-OMMT-0.5 and the neat OBC at three selected T_ss. One can see that, when 0.5 wt % of c-OMMT is introduced, the nucleation density at T_s=180°C is much higher than that of the neat OBC. On the other hand, the nucleation density of OBC/c-OMMT-0.5 at T_s=150°C is almost unchanged, as compared with that at T_s=180°C, while the number of nuclei in the neat OBC increases gradually as T_s decreases. This shows that the nucleation ability of the molecular clusters is weaker than that of c-OMMT at higher T_ss, since the amount of the molecular clusters is small. This leads to the invariant T_c of OBC/c-OMMT-0.5 when T_s is above 147°C. Moreover, because c-OMMT acts as additional thermal resistant nuclei besides the original ones in the neat OBC, the OBC/c-OMMT nanocomposites possess more thermal resistant nuclei in the melt and thus exhibit a higher T_c than the neat OBC upon cooling from 180°C. However, when T_s is low enough, a large number of molecular clusters are preserved in the melt and crystallization tends to be nucleated by the prevailing molecular clusters, resulting in denser nuclei [Figure 3(f)].

As the c-OMMT loading increases, the nucleation of c-OMMT can overwhelm that of the molecular more easily, thus the nucleation of the molecular clusters becomes insignificant even at sufficiently low T_ss, leading to the shift of $T_{I\rightarrow II}$ to lower temperature. On the other hand, the boundary temperature of D_{II} and D_{III} ($T_{II\rightarrow III}$) is hardly affected by addition of c-OMMT. Therefore, the D_{II} of OBC/c-OMMT nanocomposites is much narrower, as compared with that of the neat OBC.

The nucleation ability of c-OMMT can be further enhanced when more c-OMMT is added and thus the SN behavior is accordingly changed. The DSC cooling traces and subsequent melting traces of OBC/c-OMMT-2 at various T_ss and the variations of T_c and T_m with T_s are illustrated in Figure 4. It is observed that T_c of OBC/c-OMMT-2 is almost unchanged with lowering T_s in the whole range of T_s, indicating that D_{II} completely disappears when the c-OMMT loading reaches 2.0 wt %. The absence of D_{II} is also reported for other semicrystalline polymer nanocomposites,[27,30] which is attributed to the saturation of the thermally resistant nuclei and thus a constant nucleation density.

We also notice that the boundary temperature of D_I and D_{III} ($T_{I\rightarrow III}$) for OBC/c-OMMT-2 is 122°C, which is lower than its T_m^{end}. This means that, although there may exist some un-melted fragmental crystals, they cannot nucleate crystallization of OBC due to the high density of heterogeneous nuclei. When T_m^{end} is higher than $T_{I\rightarrow II}$ (or $T_{I\rightarrow III}$), we define the temperature range between them as D_I'. D_I' can be viewed as a subdomain of D_I, since in D_I' the subsequent crystallization is still initiated by the thermally resistant nuclei and T_c is invariant with T_s, which are the characteristics of D_I, though there exist self-nuclei of un-melted fragmental crystals in D_I'. The phenomenon that $T_{I\rightarrow II}$ is lower than T_m^{end} was also reported for some semicrystalline polymer nanocomposites in literature,[42] but D_I' was not deliberately marked off from D_I. Here D_I' is particularly emphasized, because the relative nucleation activities of the un-melted

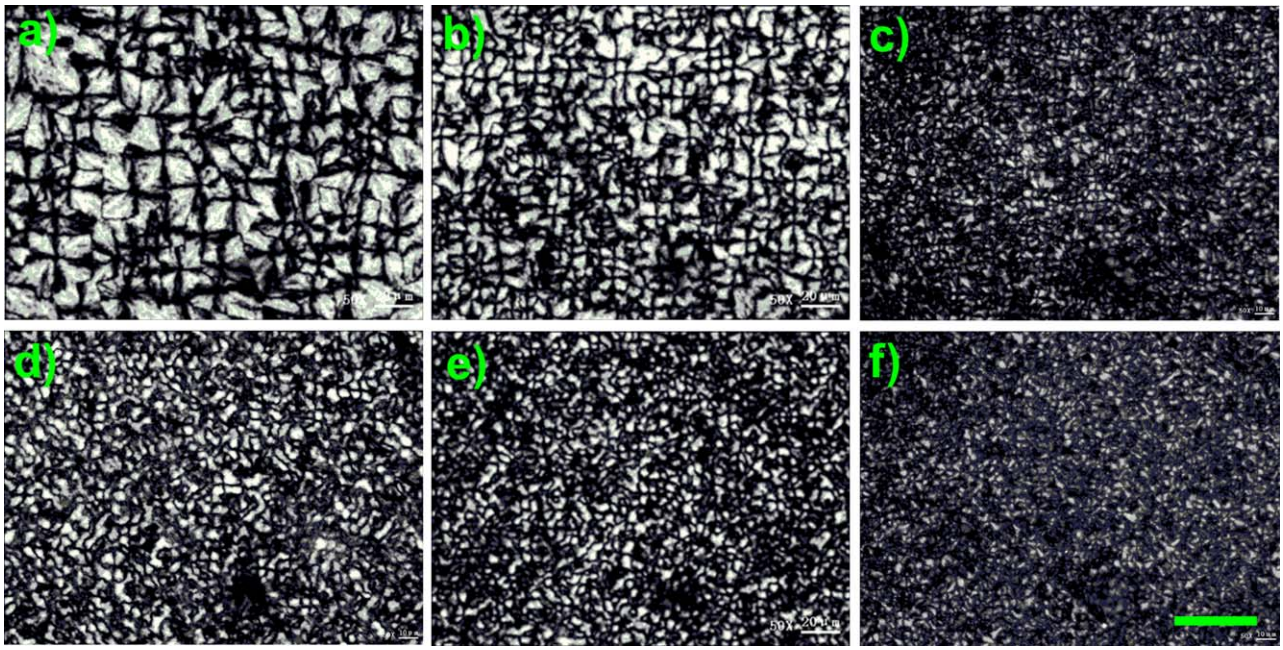

Figure 3. The final crystallization morphologies of the neat OBC after annealing at T_s= 180°C (a), 150°C (b) and 130°C (c) and of OBC/c-OMMT-0.5 after annealing at T_s= 180°C (d), 150°C (e) and 130°C (f). The scale bar in the figure is 40 μm. The thermal treatment was the same as the SN thermal protocol applied in the DSC experiment. [Color figure can be viewed in the online issue, which is available at wileyonlinelibrary.com.]

fragmental crystals (self-nuclei) and c-OMMT (heterogeneous nuclei) in D_I' and D_{II} are overturned.

Figure 5(a,b) show the DSC cooling and heating curves, respectively, for OBC/c-OMMT-3 after self-nucleation in a wide range of T_s. It can be seen that the SN behavior of this nanocomposite is quite similar to that of OBC/c-OMMT-2 because of the similar temperature ranges of D_I and D_{III}. D_{II} is not observed either and $T_{I\rightarrow III}$ is also lower than the T_m^{end} in this nanocomposite.

Comparing the temperature ranges of D_I and D_{II} of OBC/c-OMMT nanocomposites with various c-OMMT loadings (Table I), we can see that, the nucleation of the molecular clusters in the melt is first suppressed after introduction of a small amount of c-OMMT. With increasing the c-OMMT loading, the nucleation of the un-melted fragmental crystals is further covered by c-OMMT, showing that the nucleation ability of c-OMMT increases gradually with the c-OMMT loading. When the c-OMMT loading reaches 2.0 wt %, the thermally resistant nuclei are saturated and the self-nucleation domain D_{II} may completely disappear.

SN of the OBC/i-OMMT Nanocomposites

In order to compare the nucleation ability of the OMMT layers with different structures (c-OMMT and i-OMMT), we also prepared OBC/i-OMMT nanocomposites and studied their self-nucleation behaviors. Figure 6 shows the temperature ranges of different T_s domains and the variations of T_c and T_m with T_s for the OBC/i-OMMT nanocomposites containing 0.5, 1.0, and 2.0

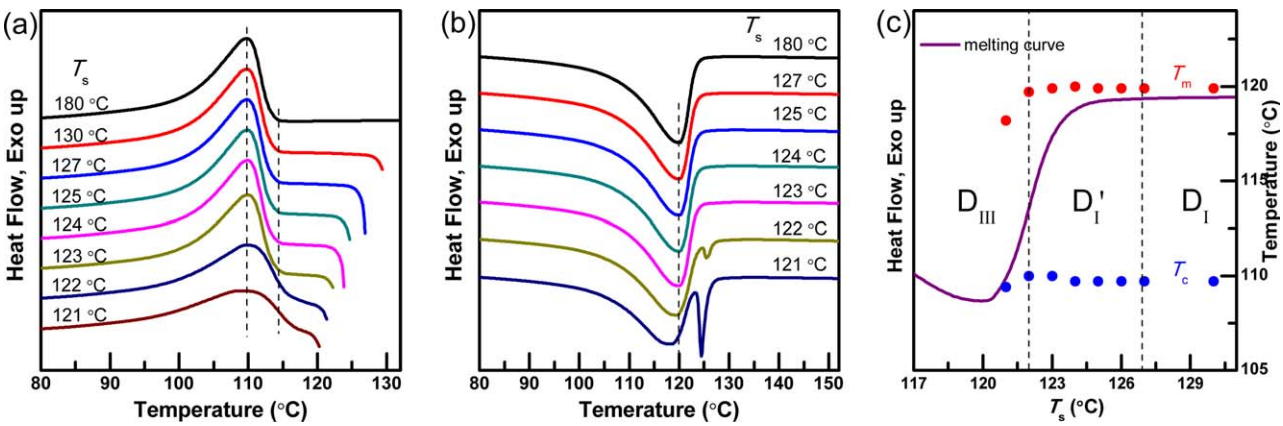

Figure 4. DSC cooling traces after self-nucleation at various T_ss (a), subsequent melting traces (b), variations of T_m and T_c with T_s and self-nucleation domains of the melting curve (divided by the vertical dashed lines) (c) of OBC/c-OMMT-2. [Color figure can be viewed in the online issue, which is available at wileyonlinelibrary.com.]

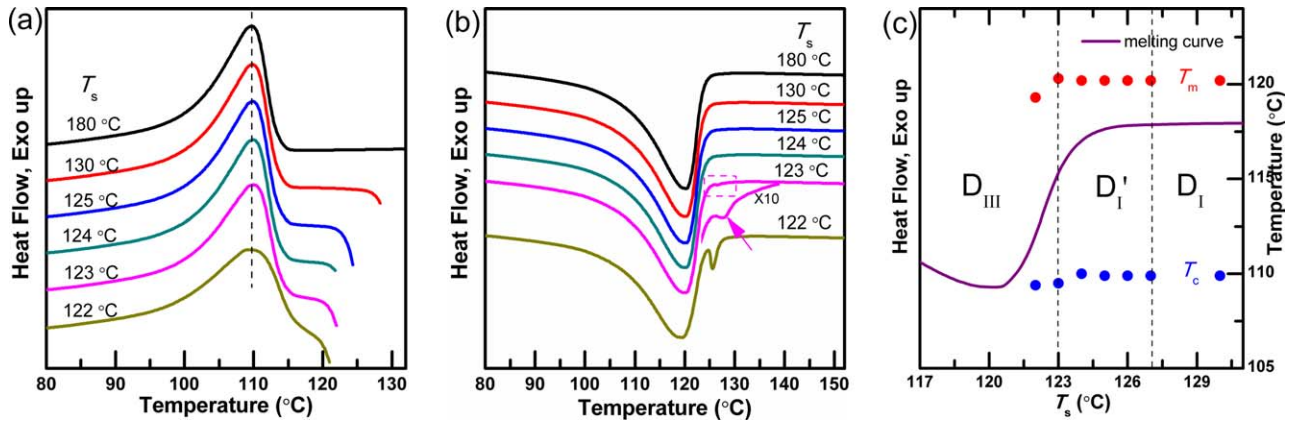

Figure 5. DSC cooling traces after self-nucleation at various T_ss (a), subsequent melting traces (b), variations of T_m and T_c with T_s and self-nucleation domains of the melting curve (divided by the vertical dashed lines) (c) of OBC/c-OMMT-3. [Color figure can be viewed in the online issue, which is available at wileyonlinelibrary.com.]

wt % i-OMMT, respectively. The related data are summarized in Table I. The $T_{I\rightarrow II}$ of OBC/i-OMMT also shifts to lower temperature and the temperature range of D_{II} becomes narrower gradually as the i-OMMT loading increases. This shows that the nucleation ability of i-OMMT is enhanced as well when more i-OMMT is added. However, we notice that the $T_{I\rightarrow II}$ of OBC/i-OMMT-1 (138°C) is obviously higher than its T_m^{end} (127°C), indicating that the molecular clusters in the melt still have a nucleation effect on the subsequent crystallization when T_s is between 138°C and 127°C. Only when the i-OMMT loading reaches 2.0 wt %, the $T_{I\rightarrow II}$ is similar to the T_m^{end} of OBC/i-OMMT-2. The DSC cooling and heating curves for OBC/i-OMMT-3 after self-nucleation at different T_ss and the variations of T_c and T_m with T_s are illustrated in Figure 7. As we can see, the $T_{I\rightarrow II}$ of OBC/i-OMMT-3 is still located nearby its T_m^{end} (125°C). This reveals that, D_I', in which the self-nuclei of un-melted fragmental crystals are present but crystallization of OBC is still initiated by the thermal resistant nuclei, cannot be observed in OBC/i-OMMT nanocomposites, even though the i-OMMT loading is as high as 3.0 wt %. The disappearance of D_I' in the OBC/i-OMMT nanocomposites shows that the thermal resistant nuclei mainly composed of i-OMMT have weaker nucleation ability than the self-nuclei of un-melted fragmental crystals. On the other hand, D_{II} can always be observed in OBC/i-OMMT nanocomposites, even in OBC/i-OMMT-3.

In order to quantify the nucleation effect, the nucleating efficiencies (NE) of c-OMMT and i-OMMT were calculated based on the following equation proposed by Müller:[28]

$$NE = \frac{T_{c,\mathrm{NA}} - T_{c,\mathrm{polymer}}}{T_{c,\mathrm{max-polymer}} - T_{c,\mathrm{polymer}}} \quad (1)$$

where $T_{c,\mathrm{NA}}$ is the peak crystallization temperature of the polymer with the nucleating agent, $T_{c,\mathrm{polymer}}$ is the peak crystallization temperature of the neat OBC and $T_{c,\mathrm{max\text{-}polymer}}$ is the maximum crystallization temperature of the ideally self-nucleated neat OBC. Figure 8 summarizes the nucleation efficiencies of two types of OMMT. It can be seen that, only in OBC/c-OMMT-2 and OBC/c-OMMT-3 the NE is above 100%. This indicates that the nucleation effect of the c-OMMT with a loading higher than 2.0 wt % is better than that of the self-nuclei. This is well consistent with the absence of D_{II} in these two nanocomposites. On the other hand, the c-OMMT

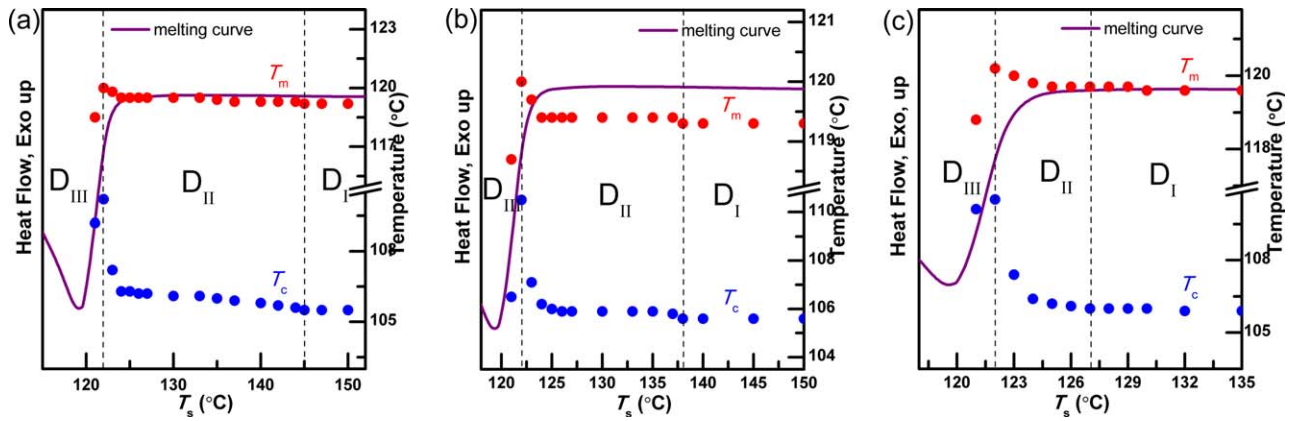

Figure 6. Variations of T_m and T_c with T_s and self-nucleation domains of the melting curve (divided by the vertical dashed lines) of OBC/i-OMMT-0.5 (a), OBC/i-OMMT-1 (b) and OBC/i-OMMT-2 (c). [Color figure can be viewed in the online issue, which is available at wileyonlinelibrary.com.]

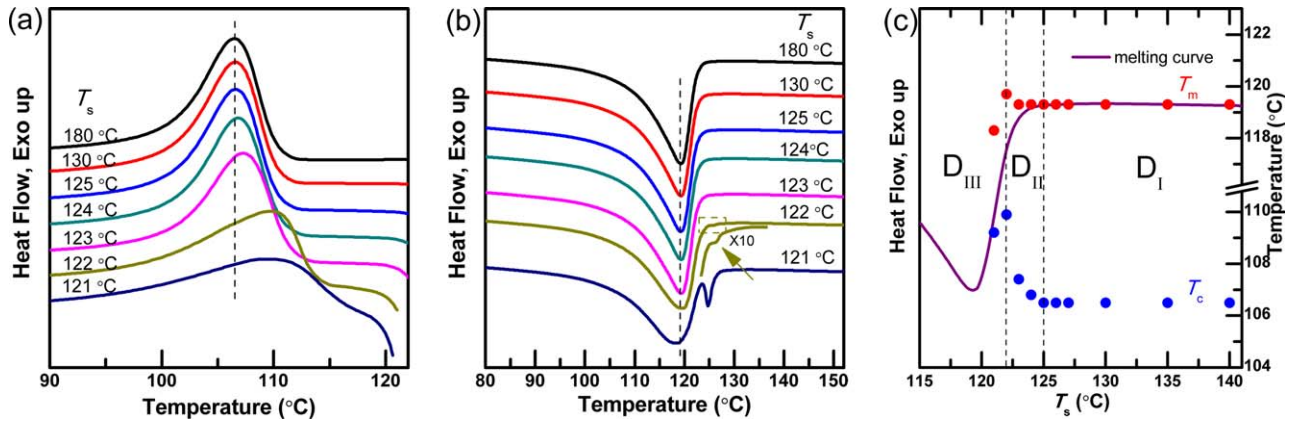

Figure 7. DSC cooling traces after self-nucleation at various T_ss (a), subsequent melting traces (b), variations of T_m and T_c with T_s and self-nucleation domains of the melting curve (divided by the vertical dashed lines) (c) of OBC/i-OMMT-3. [Color figure can be viewed in the online issue, which is available at wileyonlinelibrary.com.]

always has a much higher nucleating efficiency than i-OMMT at a given OMMT loading, showing the stronger nucleation ability of c-OMMT.

In our previous work, we found that the clay layers are densely stacked with more layers in per clay particle (8–10 layers) and a larger mean distance between the adjacent clay particles in the OBC/c-OMMT nanocomposites.[22] By contrast, the clay layers are loosely stacked in the OBC/i-OMMT nanocomposites, leading to fewer layers in per clay particle (5–7 layers) and a smaller mean distance between the adjacent clay particles. At the same clay loading the volume fraction of i-OMMT is about 1.7 times larger than that of c-OMMT in the nanocomposites.[22] As a result, the remarkable difference in the nucleation ability of c-OMMT and i-OMMT is not due to the larger surface area of c-OMMT available for nucleation, and can only ascribed to the different surface activities toward crystallization of OBC.

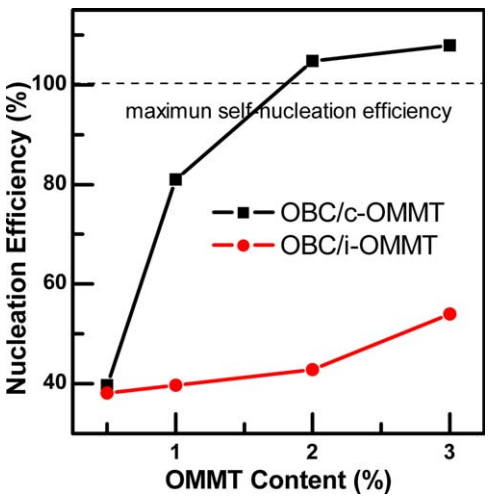

Figure 8. Nucleation efficiencies of c-OMMT and i-OMMT as nucleating agent for OBC. [Color figure can be viewed in the online issue, which is available at wileyonlinelibrary.com.]

The weaker nucleation ability of i-OMMT, as compared with that of c-OMMT, can be interpreted from following two aspects. Firstly, in the OBC/i-OMMT nanocomposites parts of the OBC segments are intercalated into the clay galleries. These segments are confined and have lower mobility. The other segments covalently linked with the intercalated segments are difficult to crystallize or nucleate on the outer surface of i-OMMT due to unfavorable entropy. Moreover, since the intercalated polymer chains with weak crystallizability and nucleation ability are always located nearby the outer surface of i-OMMT particles, which may hinder nucleation and crystallization of other polymer chains on the outer surfaces of i-OMMT. By contrast, in the OBC/c-OMMT nanocomposites there exist neither confined OBC segments nor interference effect on nucleation from the intercalated polymer chains. As a result, nucleation of OBC in the OBC/c-OMMT nanocomposites occurs more easily, resulting in a larger nucleation density.

CONCLUSION

Above results show that the SN behaviors of the neat OBC, OBC/c-OMMT and OBC/i-OMMT samples are different to some extent. There are two types of self-nuclei in the neat OBC: the molecular clusters in the melt and un-melted fragmental crystals below the T_m^{end}. Both c-OMMT and i-OMMT can suppress the nucleation activity of the molecular cluster, but only c-OMMT can overwhelm the nucleation of un-melted fragmental crystals. With increasing the OMMT loading, the $T_{I\to II}$ shifts to lower temperature and the temperature range of D_{II} becomes narrower. In the OBC/c-OMMT nanocomposites, the $T_{I\to II}$ or $T_{I\to III}$ could be lower than the T_m^{end} at high c-OMMT loadings, leading to appearance of D_I' and disappearance of D_{II}. By contrast, in OBC/i-OMMT nanocomposites D_{II} always exists and no D_I' can be observed. Furthermore, the nucleation efficiency of c-OMMT is always larger than that of i-OMMT at the same OMMT content. This stronger nucleation ability of c-OMMT can be interpreted in terms of the confinement due to intercalation and the interference effect on nucleation of the intercalated polymer chains in the OBC/i-OMMT nanocomposites.

ACKNOWLEDGMENTS

This work was supported by the National Basic Research Program of China (973 Program) (2011CB606005) and the National Natural Science Foundation of China (51073138).

REFERENCES

1. Giannelis, E. P. *Adv. Mater.* **1996**, *8*, 29.
2. Ray, S. S.; Okamoto, M. *Prog. Polym. Sci.* **2003**, *28*, 1539.
3. Zhang, X.; Loo, L. S. *Macromolecules* **2009**, *42*, 5196.
4. Krikorian, V.; Pochan, D. J. *Macromolecules* **2004**, *37*, 6480.
5. Liu, X. H.; Wu, Q. J.; Berglund, L. A. *Polymer* **2002**, *43*, 4967.
6. Ou, C. F.; Ho, M. T.; Lin, J. R. *J. Polym. Res.-Taiwan* **2003**, *10*, 127.
7. Huang, J. W. *J. Appl. Polym. Sci.* **2008**, *110*, 2195.
8. Tong, Z. Z.; Zhou, B.; Huang, J.; Xu, J. T.; Fan, Z. Q. *Compos. Sci. Technol.* **2013**, *85*, 111.
9. Xu, J. T.; Wang, Q.; Fan, Z. Q. *Eur. Polym. J.* **2005**, *41*, 3011.
10. Xu, J. T.; Zhao, Y. Q.; Wang, Q.; Fan, Z. Q. *Polymer* **2005**, *46*, 11978.
11. Arriola, D. J.; Carnahan, E. M.; Hustad, P. D.; Kuhlman, R. L.; Wenzel, T. T. *Science* **2006**, *312*, 714.
12. Wang, H. P.; Khariwala, D. U.; Cheung, W.; Chum, S. P.; Hiltner, A.; Baer, E. *Macromolecules* **2007**, *40*, 2852.
13. Khariwala, D. U.; Taha, A.; Chum, S. P.; Hiltner, A.; Baer, E. *Polymer* **2008**, *49*, 1365.
14. Jin, J.; Du, J. A.; Xia, Q. H.; Liang, Y. R.; Han, C. C. *Macromolecules* **2010**, *43*, 10554.
15. Li, S.; Register, R. A.; Weinhold, J. D.; Landes, B. G. *Macromolecules* **2012**, *45*, 5773.
16. Tong, Z. Z.; Huang, J.; Zhou, B.; Xu, J. T.; Fan, Z. Q. *Macromol. Chem. Phys.* **2013**, *214*, 605.
17. Tong, Z. Z.; Xu, J. T.; Xia, S. J.; Fan, Z. Q. *Polym. Int.* **2013**, *62*, 228.
18. Tong, Z. Z.; Zhou, B.; Huang, J.; Xu, J. T.; Fan, Z. Q. *Macromolecules* **2014**, *47*, 333.
19. Yoon, J. T.; Jo, W. H.; Lee, M. S.; Ko, M. B. *Polymer* **2001**, *42*, 329.
20. Yoon, P. J.; Hunter, D. L.; Paul, D. R. *Polymer* **2003**, *44*, 5323.
21. Hotta, S.; Paul, D. R. *Polymer* **2004**, *45*, 7639.
22. Tong, Z. Z.; Zhou, B.; Huang, J.; Xu, J. T.; Fan, Z. Q. *RSC Adv.* **2014**, *4*, 15678.
23. Sabino, M. A.; Ronca, G.; Müller, A. J. *J. Mater. Sci.* **2000**, *35*, 5071.
24. Cavallo, D.; Gardella, L.; Portale, G.; Müller, A. J.; Alfonso, G. C. *Polymer* **2013**, *54*, 4637.
25. Cavallo, D.; Gardella, L.; Portale, G.; Müller, A. J.; Alfonso, G. C. *Polymer* **2014**, *55*, 137.
26. Yu, L.; Wu, T.; Chen, T.; Yang, F.; Xiang, M. *Thermochim. Acta* **2014**, *578*, 43.
27. Trujillo, M.; Arnal, M. L.; Müller, A. J.; Laredo, E.; Bredeau, S.; Bonduel, D.; Dubois, P. *Macromolecules* **2007**, *40*, 6268.
28. Müller, A. J.; Arnal, M. L.; Trujillo, M.; Lorenzo, A. T. *Eur. Polym. J.* **2011**, *47*, 614.
29. Trujillo, M.; Arnal, M. L.; Müller, A. J.; Mujica, M. A.; Urbina de Navarro, C.; Ruelle, B.; Dubois, P. *Polymer* **2012**, *53*, 832.
30. Pucciariello, R.; Villani, V.; Giammarino, G. *J. Polym. Res.* **2011**, *18*, 949.
31. Müller, A. J.; Arnal, M. L.; López-Carrasquero, F. *Macromol. Symp.* **2002**, *183*, 199.
32. Müller, A. J.; Balsamo, V.; Arnal, M. L. *Adv. Polym. Sci.* **2005**, *190*, 1.
33. Castillo, R. V. N.; Müller, A. J.; Raquez, J.-M.; Dubois, P. *Macromolecules* **2010**, *43*, 4149.
34. Pan, Y. Y.; Yu, X. F.; Shi, T. F.; An, L. J. *Chin. J. Polym. Sci.* **2010**, *28*, 347.
35. Huang, C. L.; Jiao, L.; Zeng, J. B.; Zhang, J. J.; Yang, K. K.; Wang, Y. Z. *J. Phys. Chem. B* **2013**, *117*, 10665.
36. Fillon, B.; Wittmann, J. C.; Lotz, B.; Thierry, A. *J. Polym. Sci. Part B: Polym. Phys.* **1993**, *31*, 1383.
37. Flory, P. J.; Vrij, A. *J. Am. Chem. Soc.* **1963**, *85*, 3548.
38. Müller, A. J.; Lorenzo, A. T.; Arnal, M. L.; de Fierro, A. B.; Abetz, V. *Macromol. Symp.* **2006**, *240*, 114.
39. Gao, H.; Vadlamudi, M.; Alamo, R. G.; Hu, W. B. *Macromolecules* **2013**, *46*, 6498.
40. Reid, B. O.; Vadlamudi, M.; Mamun, A.; Janani, H.; Gao, H.; Hu, W. B.; Alamo, R. G. *Macromolecules* **2013**, *46*, 6485.
41. Wunderlich, B. *Thermochim. Acta* **2011**, *522*, 2.
42. Balsamo, V.; Paolini, Y.; Ronca, G.; Müller, A. J. *Macromol. Chem. Phys.* **2000**, *201*, 2711.